# Energetic and Structural Characterizations of the PET–Water Interface as a Key Step in Understanding Its Depolymerization

Pierre Fayon, Julien Devémy, Constance Emeriau-Viard, Karine Ballerat-Busserolles, Florent Goujon, Alain Dequidt, Alain Marty, Patrice Hauret, Patrice Malfreyt

# Energetic and Structural Characterizations of the PET-Water Interface as a Key-step in Understanding its Depolymerization

Pierre Fayon,[*,†] Julien Devémy,[†] Constance Emeriau-Viard,[‡] Karine Ballerat-Busserolles,[†] Florent Goujon,[†] Alain Dequidt,[†] Alain Marty,[¶] Patrice Hauret,[‡] and Patrice Malfreyt[*,†]

†*Université Clermont Auvergne, Clermont Auvergne INP, CNRS, Institut de Chimie de Clermont-Ferrand, F-63000 Clermont-Ferrand, France*

‡*Manufacture Française des Pneumatiques Michelin, 23, Place des Carmes, 63040, Clermont-Ferrand, France*

¶*Carbios, Parc Cataroux, Batiment B80, 8 rue de la Grolière 63100 Clermont-Ferrand, France*

E-mail: pierre.fayon@uca.fr; patrice.malfreyt@uca.fr

Phone: +33 (0)473407204

**Abstract**

We report molecular simulations of the interaction between poly(ethylene terephthalate) (PET) surfaces and water molecules with a short-term goal to better evaluate the different energy contributions governing the enzymatic degradation of amorphous PET. After checking that the glass transition temperature, density, entanglement mass and mechanical properties of an amorphous PET are well reproduced by our molecular model, we extend the study to the extraction of a monomer from the bulk surface in different environments *i.e* water, vacuum, dodecane and ethylene glycol. We complete this energetic characterization by the calculation of the work of adhesion of PET surfaces with water and dodecane molecules and by the determination of the contact angle of water droplets. These calculations are compared with experiments and should help us to better understand the enzymatic degradation of PET from both the thermodynamic and molecular viewpoints.

# 1 Introduction

Poly(ethylene terephthalate) (PET) is a polyester plastic, with an annual production of 98 million tons in 2021, of which only 3% is recycled.[1] PET is a lightweight, economical and multipurpose material, being used in various applications such as making of bottles to contain edibles, trays, sportswear, clothing, and many other products. Looking at the wide array of usable products made from recycled PET material, it is the largest volume being recycled. The recycling process minimizes the effects on the environment, the main methods for PET recycling are via mechanical recycling, chemical recycling and enzyme catalysis. In the case of mechanical recycling, the plastic scrap is sorted, cleaned, washed and other impurities are removed, it is grounded into flakes and sent to the extrusion machine for melting. After melting, the final material, plastic granules, can be used further to produce different products.[2] One of the main problems with this method is that the average molecular weight of the polymer drops and therefore there is a loss in its mechanical properties.[3]

For the chemical recycling process, the plastic waste is shredded into powder and left for the chemical process (e.g hydrolysis, alcoholysis, glycolysis, etc[4]) to melt. The obvious disadvantages of this method are the use of additional chemicals and high temperature to achieve an efficient process.[5] In the early 2000's a new bio technology method based on enzyme catalysis appeared with many advantages compared with classical mechanical and chemical processes.[6] The main ones are the action of an enzyme operating under mild conditions with low energy input,[6] and the enzyme selectivity avoiding intensive sorting via hydrolysis catalyze primary by a class of enzyme called cutinase.

The degradation of PET has been reported for members of the cutinase,[7] lipase,[8] esterase,[9] and petase enzymes.[10] Because of its synthetic nature, the biodegradation of PET by enzymatic reactions is difficult, which results in slow enzymatic rate toward this polymer.[11] Hence, protein engineering approach has been to increase the affinity of cutinase to PET and its ability to hydrolyze it.[12,13] In 2016, a new enzyme has been discovered by Yosida et al.[14] They found a new species of bacteria *Ideonella sakaiensis* outside a bottle-recycling facility which could break down the plastic by using two enzymes to hydrolyze PET converting it into basic building blocks; terephthalic acid and ethylene glycol. Since then, interest in developing new enzymes capable of degrading PET by protein engineering has been increased.[12,15] Hopefully, enzyme technology could be applicable in large scale and improving green industries especially for plastic recycling. The limiting factor with enzyme depolymerization, is due to the fact that the activity is optimum at temperatures close to the glass transition temperature, which is around 75° for amorphous PET.[16] Hence, protein engineering studies have been performed to increase thermal stability of the cutinases.[7]

According to these studies, the degradation of PET by an enzyme, is increased when chain flexibility increases upon heating in amorphous regions and consequently becoming more accessible to the enzyme catalytic site.[17] Hence, the flexibility, spatial configuration of polymer chains, and presence of solvent media would be the major factors in this regard. In general, converting PET materials to terephtalic acid and ethylene glycol under

mild conditions could be achieved through further studies and needs more activities until the degradation efficiency get increased.[18] To understand the impact of the polymer structure, mechanical and thermodynamic properties at a molecular level, the use of molecular dynamics (MD) simulation could provide a deep understanding of the phenomena taking place at the enzyme-polymer-solvent interface.

A large number of theoretical studies have been carried out on the degradation process of PET by an enzyme, mainly via docking,[19] QM/MM methods,[20–23] molecular simulations[24,25] and recently by machine-learning[26] to engineer an active PET-hydrolase. Currently the molecular mechanism of PET degradation by the enzyme is far from being resolved. One of the process hypothesis is that the enzyme finds the end of a chain and starts the degradation monomer by monomer on the same chain. In that case, it means the interaction between the enzyme and the polymer is more favorable than the interaction of polymer-polymer and polymer-solvent. For this reason, we focus here on the PET-water interaction which can be expressed in different properties such as work of adhesion and contact angle. This study therefore precedes any study that explicitly considers the role of the enzyme. The main objective of our work, is to check if it is energetically favorable to pull out a chain from the bulk into the solvent. As mentioned above, we do not take the route of considering explicitly the enzyme even if we plan to mimic its action and to get an idea of how it might work in a future work. In this paper, we model a slab of PET in contact with various solvents, and we extract one of its chain from the bulk. We simulate a chain's extraction by calculating the potential of mean force (PMF) with an umbrella-sampling (US) methodology. We complete this energetic characterization of extraction by investigating structural properties. This leads us to have a deeper look at the interfacial region. The knowledge of the local properties at the interface is an essential step toward the development of new procedures for polymer recycling via enzyme catalysis. The structuration of the molecules at the interface is governed by a balance between specific interactions that can be described through van der Waals, electrostatic, and hydrogen bond energy. The objective of this study is to propose a plausible

molecular model of a PET bulk, elucidate its structural organization on a molecular level, and explore properties of water at the surface. The present study may shed some lights on the nature of the PET-water interfacial region in terms of interactions and structural arrangements which may help us to better understand the enzymatic degradation of these materials.

# 2 Methods

## 2.1 Experiments

In the present study, we report experimental results on the glass transition temperature and the contact angle formed by a drop of water on an amorphous PET surface. The thermal analysis was realized using a Thermogravimetric Balance (TGA/DSC) DSC 3+ from Mettler Toledo. The sample is placed in a crucible, with an average weight of 25 mg, this crucible was installed on the thermobalance together with a reference one fully empty, in order to proceed the experiment as a differential measurement. Under each crucible, thermocouples allow to measure heat flux signal together with sample weight loss, indicating roughly any thermic effect associated to weight loss. The used thermal profile was the following: first isotherm was measured at 298.15 K for 1 min, in order to reach equilibrium in the sample. Then the temperature of the sample was increased from 298.15 K up to 623.15 K with a constant scanning rate of $20\,\mathrm{K\,min^{-1}}$, follow by an isotherm at 623.15 K for 5 min, a cooling down to 298.15 K with a constant scanning rate of $30\,\mathrm{K\,min^{-1}}$, and finally the temperature of the sample is increased from 298.15 K up to 623.15 K with a constant scanning rate of $20\,\mathrm{K\,min^{-1}}$. The characterization of the thermal properties of the PET samples is carried out on the second heating which makes it possible to characterize the material by freeing itself from the thermal past of the sample. In order to get more precise thermograms, DSC experiments were also performed on the sample. A differential scanning calorimeter DSC evo from SETARAM was used to measure thermal flux versus temperature on similar samples.

The average mass introduced in the crucible is 10 mg. The scanning rate used was 20 K min$^{-1}$ and the range of temperature considered was from ambient up to 573 K. These conditions allow to determine glass transitions and heat effect associated to the degradation of the sample.

From an experimental point of view, if we want to calculate the work of adhesion between a solid and a liquid, we can measure the contact angle of a droplet onto a planar surface of the solid, if we know the surface tension of the liquid. The determination of the surface tension $\gamma_{LV}$ can be acquired with different methods, using a tensiometer[27] or using the pendant drop method.[28] Experimentally we can determine the surface tension of the solid $\gamma_{SV}$, if we know the surface tension of three different liquids as well as the components of their surface tensions,[29] then it is easy to determine $\gamma_{SL}$ and $\gamma_{SV}$.

Contact angles were assessed experimentally, on the amorphous PET provided by the supplier Goodfellow. Contact angles were performed at constant and controlled temperature using a dataphysics OCA 15 Pro goniometer equipped with a thermostatic chamber and a Peltier element, allowing measurements for temperature ranging from 283 K up to 373 K. The contact angle between a solvent and the polymer surface was determined using the sessile drop method. The liquid droplets were photographed by a camera with a resolution of 752 $\times$ 480 pixels and an optical distortion below 0.05%. The SCA20 (Dataphysics Instruments GmbH) software was used to automate the measurements, and the contact angle were determined from analysis of the shadow image of the drop. The detection limit of the angle is 8°. Contact angles were determined by depositing 15 µL droplets on the polymer surface. Four droplets were placed simultaneously with enough spacing to avoid overlapping. In order to limit the evaporation problems of the droplet during experiment, the exact same procedure was observed for each temperature: A small quantity of the fluid to be measured was placed in the thermostatic chamber before starting the experiments. The objective is to reach vapor-liquid equilibrium, so that the droplets remain on the solid surface and their volumes change slowly enough to allow good precision of measurements.

## 2.2 Description of the force fields

We used the PCCF+ (Polymer Consistent Force Field-enhanced) force field developed by MedeA,[30] to describe the PET. The PCFF+ force field is an improved version of the PCFF force field which is a member of the Consistent Force Field (CFF) family.[31,32] This class II force field has the following functional form:

$$
\begin{aligned}
\mathcal{U} = & \sum_{Bonds} \left( k_2 \left( r_{ij} - r_0 \right)^2 + k_3 \left( r_{ij} - r_0 \right)^3 + k_4 \left( r_{ij} - r_0 \right)^4 \right) \\
& + \sum_{Angles} \left( E_a + E_{bb} + E_{ba} \right) \\
& + \sum_{Dihedrals} \left( E_d + E_{mbt} + E_{ebt} + E_{at} + E_{aat} + E_{bb13} \right) \\
& + \sum_{Impropers} \left( E_i + E_{aa} \right) \\
& + \sum_{Nonbonded\ atoms} \frac{q_i \, q_j}{4\pi \, \epsilon_0 \, r_{ij}} \\
& + \sum_{Nonbonded\ atoms} \epsilon_{ij} \left[ 2 \left( \frac{\sigma_{ij}}{r_{ij}} \right)^9 - 3 \left( \frac{\sigma_{ij}}{r_{ij}} \right)^6 \right],
\end{aligned}
\tag{1}
$$

where $E_a = K_2(\theta - \theta_0)^2 + K_3(\theta - \theta_0)^3 + K_4(\theta - \theta_0)^4$ is the angle term, $E_{bb} = M(r_{ij} - r_1)(r_{jk} - r_2)$ is a bond-bond term, and $E_{ba} = N_1(r_{ij} - r_1)(\theta - \theta_0) + N_1(r_{jk} - r_2)(\theta - \theta_0)$ is a bond-angle term, $\theta_0$ is the equilibrium angle and $r_1$ and $r_2$ are the equilibrium bond lengths. The terms of the dihedral potential are, the dihedral term $E_d = \sum_{n=1}^{3} K_n \left[ 1 - cos(n\phi - \phi_n) \right]$, the middle-bond-torsion term $E_{mbt} = (r_{jk} - r_2) \left[ A_1 cos(\phi) + A_2 cos(2\phi) + A_3 cos(3\phi) \right]$, the end-bond-torsion term $E_{ebt} = (r_{ij} - r_1) \left[ B_1 cos(\phi) + B_2 cos(2\phi) + B_3 cos(3\phi) \right] + (r_{kl} - r_3) [C_1 cos(\phi) + C_2 cos(2\phi) + C_3 cos(3\phi)]$, the angle-torsion term $E_{at} = (\theta_{ijk} - \theta_1) \left[ D_1 cos(\phi) + D_2 cos(2\phi) + D_3 cos(3\phi) \right] + (\theta_{jkl} - \theta_2) \left[ E_1 cos(\phi) + E_2 cos(2\phi) + E_3 cos(3\phi) \right]$, the angle-angle-torsion term $E_{aat} = M(\theta_{ijk} - \theta_1)(\theta_{jkl} - \theta_2) cos(\phi)$, and the bond-bond-13 term $E_{bb13} = N(r_{ij} - r_1)(r_{kl} - r_3)$, with $\theta_1$ and $\theta_2$ are equilibrium angles and $r_1$, $r_2$ and $r_3$ are equilibrium bond lengths. The improper terms

are, the improper term $E_i = K\left[\frac{\chi_{ijkl}+\chi_{kjli}+\chi_{ljik}}{3} - \chi_0\right]^2$, The three $\chi$ terms are an average over three out-of-plane angles. Finally $E_{aa} = M_1(\theta_{ijk} - \theta_1)(\theta_{kjl} - \theta_3) + M_1(\theta_{ijk} - \theta_1)(\theta_{ijl} - \theta_2) + M_1(\theta_{ijl} - \theta_2)(\theta_{kjl} - \theta_3)$ is an angle-angle term. The Lennard-Jones parameters between pairs of different atoms are obtained from the sixth-power combination rules $\epsilon_{ij} = \frac{2\sqrt{\epsilon_i\epsilon_j}\sigma_i^3\sigma_j^3}{\sigma_i^6+\sigma_j^6}$, and $\sigma_{ij} = \left(\frac{1}{2}(\sigma_i^6 + \sigma_j^6)\right)^{\frac{1}{6}}$.

The employed water model is the TIP4P/2005[33] parameterized with a 12-6 form for the Lennard-Jones potential and using the Lorentz/Berthelot mixing rules. We showed earlier that the PCFF+ force field uses a 9-6 form for the Lennard-Jones potential. Since we are using models with different mixing rules, we select to use the Lorentz-Berthelot mixing rules for the cross-term between water molecules and polymers.

## 2.3 Calculation of the work of adhesion

The contact angle, given by Young-Dupre's equation,[34] is expressed by

$$cos\,\theta = \frac{\gamma_{\mathrm{SV}} - \gamma_{\mathrm{SL}}}{\gamma_{\mathrm{LV}}}, \tag{2}$$

where $\theta$ is the contact angle of the liquid onto the surface, and $\gamma_{\mathrm{SL}}$, $\gamma_{\mathrm{SV}}$, and $\gamma_{\mathrm{LV}}$ are the solid-liquid, the solid-vapor and the liquid-vapor interfacial tensions respectively. A contact angle less than $90^o$ indicates that the the wetting of the surface by the liquid is favorable. If $\theta$ is superior than $90^o$ then the liquid try to minimize its contact with the surface by forming a compact liquid droplet.

The thermodynamic work of adhesion between a solid and a liquid $W_{\mathrm{SL}}$, is the work required to separate two phases in contact, at equilibrium state and is related to surface free energies by the Dupré equation :

$$W_{\mathrm{SL}} = \gamma_{\mathrm{LV}} + \gamma_{\mathrm{SV}} - \gamma_{\mathrm{SL}}. \tag{3}$$

Combining eq (2) and eq (3) we can obtain a relation between the contact angle the liquid-

vapor interfacial tension and the work of adhesion:

$$W_{\mathrm{SL}} = \gamma_{\mathrm{LV}}(1 + \cos\theta). \tag{4}$$

A rise in the interfacial attraction results in an increase in the work of adhesion, or in an other term when $\gamma_{\mathrm{SL}}$ tends to zero. This quantity, $W_{\mathrm{SL}}$ may be either positive or negative; if positive the two surfaces will bond and the higher the value of $W_{\mathrm{SL}}$ the stronger the adhesion.

It is possible to calculate directly the work of adhesion using the Free Energy Perturbation method (FEP), also referred as the dry-surface method.[35] If we consider a classical system within $N$ identical particles of mass $m$, coordinates $\mathbf{r}^N$ and momenta $\mathbf{p}^N$; the Helmholtz free energy $F$ is related to the partition function $Q_{NVT}$ in the $NVT$ ensemble by the following expression :

$$\begin{aligned} F &= -\frac{1}{\beta}\ln Q_{\mathrm{NVT}} \\ &= -\frac{1}{\beta}\ln\left(\frac{1}{h^{3N}N!}\int\int d\mathbf{r}^N d\mathbf{p}^N \exp\left(-\beta\mathcal{H}(\mathbf{r}^N,\mathbf{p}^N)\right)\right) \\ &= -\frac{1}{\beta}\ln\left(\frac{1}{\Lambda^{3N}N!}\int d\mathbf{r}^N \exp\left(-\beta\mathcal{U}(\mathbf{r}^N)\right)\right), \end{aligned} \tag{5}$$

where $\beta = \frac{1}{k_B T}$ is the inverse temperature and $h$ is the Planck constant. The total Hamiltonian in eq (5) can be written as the sum of the kinetic and potential energies of the system. Suppose that the potential energy $\mathcal{U}(\mathbf{r}^N)$ is independent of the velocities, the double integral in eq (5) can be separated in two integrals, one over the positions and one over the momenta. This latter can be written in terms of the de Broglie thermal wavelength, $\Lambda$. The resulting expression of the Helmholtz free energy is given by eq (6).

$$\begin{aligned} \Delta F = F^{(1)} - F^{(0)} &= -\frac{1}{\beta}\ln\frac{Q^{(1)}_{\mathrm{NVT}}}{Q^{(0)}_{\mathrm{NVT}}} \\ &= -\frac{1}{\beta}\ln\left\langle \exp\left[-\beta\left(\mathcal{H}^{(1)}(\mathbf{r}^N,\mathbf{p}^N) - \mathcal{H}^{(0)}(\mathbf{r}^N,\mathbf{p}^N)\right)\right]\right\rangle_0, \end{aligned} \tag{6}$$

where $\mathcal{H}^{(1)}(\mathbf{r}^N, \mathbf{p}^N)$ and $\mathcal{H}^{(0)}(\mathbf{r}^N, \mathbf{p}^N)$ are the total Hamiltonian of the target and reference systems, respectively. The expression of eq (6) is the fundamental expression of the FEP [36–39] methodology. The reference system labelled as (0) is defined by the interaction between the solid and liquid phases characterized by $\gamma_{\mathrm{SL}}$. The target system (1) is then formed by a solid phase and a liquid phase in equilibrium with their vapor. Both phases no longer interact with each other and lead to two interfacial tensions $\gamma_{\mathrm{LV}}$ and $\gamma_{\mathrm{SV}}$. We can describe the transformation with the following expression :

$$\Delta F = \mathcal{A} \times W_{\mathrm{SL}} = \mathcal{A} \times \Big( \gamma_{\mathrm{LV}} + \gamma_{\mathrm{SV}} - \gamma_{\mathrm{SL}} \Big), \tag{7}$$

where $\mathcal{A}$ is the surface area of the solid. Since the transformation does not involve changes in mass and temperature, it results that the kinetic term obtained through the de Broglie thermal wavelength cancels out. As a consequence, we replace the Hamiltonian by the potential energy $\mathcal{U}(\mathbf{r}^N)$ and we will omit the dependence of $\mathcal{U}$ on the positions $\mathbf{r}^N$ for simplicity of notation.

To improve the convergence of the calculation and to promote overlaps between consecutive steps, the calculation of the free energy difference $\Delta F$ between two states (0) and (1) is split into $N_w$ intermediate contiguous states or windows defined by a coupling constant $\lambda_i$. The potential energy is a function of $\lambda_i$ as described by equation (8)

$$\mathcal{U}(\lambda_i) = \lambda_i \, \mathcal{U}(\lambda_{N_w}) + (1 - \lambda_i) \mathcal{U}(\lambda_1) \tag{8}$$

where $0 \leq \lambda_i \leq 1$, $\lambda_1 = 0$ and $\lambda_{N_w} = 1$. Eq (5) can be rewritten in the context of the calculation over consecutive states $(i)$ and $(i+1)$

$$\begin{aligned} \Delta F = F^{(1)} - F^{(0)} &= \sum_{i=1}^{N_w - 1} \Delta F(\lambda_i) \\ &= -\frac{1}{\beta} \sum_{i=1}^{N_w - 1} \ln \Big\langle \exp \Big[ -\beta \Big( \mathcal{U}(\lambda_{i+1}) - \mathcal{U}(\lambda_i) \Big) \Big] \Big\rangle_{\lambda_i} \end{aligned} \tag{9}$$

The perturbations can be performed in both directions ("double-wide sampling") with $N_w$ windows over the entire simulation. The difference between the forward ($\Delta\lambda = \lambda_{i+1} - \lambda_i$) and backward ($\Delta\lambda = \lambda_{i-1} - \lambda_i$) simulations gives a lower-bound estimate of the error in the calculations. The transformation from state ($i$) to state ($i+1$) is achieved by changing the interactions between the solid and the liquid molecules and keeping identical the solid-solid and liquid-liquid interactions. This is done by applying the following rules to the cross interactions between the atoms of the solid and liquid phases as :

$$\varepsilon_{SL}(\lambda_i) = (1 - \lambda_i)\sqrt{\varepsilon_{SS}\varepsilon_{LL}}, \tag{10}$$

where $S$ and $L$ represent atoms of the solid and liquid phases, respectively. The removal of the interactions between the solid and liquid atoms can lead to instabilities when the coupling parameter $\lambda_i$ approaches 0. A solution has been proposed by Beutler et al,[40] it consists of modifying the Lennard-Jones potential as :

$$U_{\mathrm{LJ}}(r_{ij}, \lambda_i) = (1 - \lambda_i)\varepsilon_{ij}\left[\frac{1}{\left(\alpha(\lambda_i)^2 + \left(\frac{R_{min,ij}}{r_{ij}}\right)^6\right)^2} - \frac{1}{\alpha(\lambda_i)^2 + \left(\frac{R_{min,ij}}{r_{ij}}\right)^6}\right], \tag{11}$$

where $\alpha$ was taken to 0.1. As $\lambda_i$ is 0, the solid and liquid molecules interact through the full strength of the Lennard-Jones potential. As $\lambda_i$ approaches 1, the Lennard-Jones potential is modified by a soft-core interaction $\alpha\lambda_i^2$.

## 2.4 Calculation of the contact angle by molecular simulations

MD simulation method has also been used to study wetting through the use of a liquid nanodroplet in contact with a surface.[41–45] This technique is similar to the sessile drop technique used in experiments but on a different size scale. This calculation is done by building a droplet of the liquid of interest, and then equilibrating the system. Once the

equilibration is achieved, the shape of the liquid onto the the surface is examined and the contact angle is deduced. However, it is well known from MD simulation that the contact angle of droplets depends largely on their size[42,46,47] which is the order of few nanometers. Therefore, it is necessary to consider the droplet size. The modified Young's equation[48,49] that takes into account the size dependence is given by

$$cos\,\theta_{\mu} = cos\,\theta - \frac{\tau}{\gamma_{\mathrm{LV}}}\frac{1}{r_{dr}}, \tag{12}$$

where $\theta_{\mu}$ is the contact angle of the microscopic droplet, $\theta$ is the contact angle of eq (2), $\tau$ is the line tension, and $r_{dr}$ is the radius of a contact surface between the droplet and the surface. Hirvi and Pakkanen reported the droplet size dependence of the contact angle of water on polymer surfaces with frozen molecular motion.[42] However, calculating $\theta_{\mu}$ at molecular level is not an easy task. Different methods to fit the outline of a droplet onto a spherical shape have been proposed. One method for calculating the contact angle is by first defining a z-axis passing through the center of mass of the droplet, perpendicular to the surface.[50] Then, the droplet is divided into slabs parallel to the surface. For each slab, the horizontal density profile is calculated and for each slab a drop radius is associated as a function of a chosen density. Another method is based on the relation between the average height of the center of mass of the water droplet and contact angle.[51] In this paper, we determined the contact angle by fitting a spherical cap on the water density by using maximum likelihood method.[52]

# 3 Computational details

All the calculations were performed with LAMMPS software.[53] The Velocity-Verlet integrator was used to integrate the equations of motion using a time step of 1 fs. The SHAKE algorithm was used to constrain the bonds and the angle of the water molecules. The temperature and pressure for NVT and NPT simulations were controlled with a Nosé-Hoover thermostat and barostat,[54] with a damping of $100\delta t$ for the thermostat and $500\delta t$ for the

barostat. The cutoff radius for van der Waals interactions was set to 15 Å, and the coulombic interaction were calculated using the PPPM solver with a precision of $10^{-4}$. The periodic boundary conditions were applied in the three directions. All the MD simulations were performed at 300 K and 1 atm. The simulation systems were generated using the PACKMOL package.[55]

The PMF calculations has been performed by using the umbrella sampling (US) method, and the COLVARS module package.[56] The PMF was defined as the distance between the hydrogen at the end of the chain and the centers-of-mass of all the other chains. In the US method, the trajectory desired for the considered molecule is divided into windows. The position of the molecule is restrained by a potential to sample within each window. This gives access to the free energy profile along the reaction coordinate. If the energy is positive then the reaction considered is not favorable. We used this method on a slab of amorphous PET, and extracted the same chain for 10 Å (which is about the size of one monomer, the total length of the chain being about 150 Å ), into different environments. We chose, water, vacuum, dodecane and ethylene glycol. These four solvents, represent various environments from a chemical point of view. The enzyme is made to work in aqueous media, which is why the first solvent of choice is water, however during the degradation of the polymer more and more ethylene glycol is produced, and it motivated us to invertigate the effect of this solvent on the degradation process. As these two solvents are hydrophilic, we want to compare them with a hydrophobic solvent, so we studied the case with dodecane. Finally, we performed the same simulations in vacuum as our reference. The PMF was run in the NVT ensemble,using 100 steps, (each one equal to 0.1 Å of perturbation), with 250 ps of acquisition. We only performed these simulations on amorphous polymer, since experimentally there is no sign of degradation onto the crystalline part of the PET. We adopted the convention that the Gibbs free energy is zero at the beginning of the simulation. In other words it is zero at the starting point of the equilibrated system.

# 4 Results and discussion

The result section consists of three parts. First, we focus on the physical properties of the PET alone to validate our force field and system size. Second, we extract a PET monomer from the bulk using a potential of mean force to determine the energy needed for a biological system to access a single chain from the bulk. In the final part, we proceed to analyse the interfacial region by calculating structural and energetic properties.

## 4.1 Entanglement, density, glass transition temperature, and mechanics properties

We start this study with reference properties available in the literature,[16,57–60] density and the glass transition temperature ($T_g$) which are the most common properties to look at when studying polymers. To calculate the density and the $T_g$ of our model, eight independent structures consisting of 12 chains of 15 monomers each were generated. Experimentally, the density of amorphous PET at 300 K is between 1.333 and 1.342 g cm$^{-3}$ [16,57] with a glass transition temperature of 342 K.[60] These values may vary slightly if the PET samples have been subjected to treatments (temperature, pressure...), and generally the $T_g$ of PET varies between 343 K and 358 K.[61]

For each of the eight structures generated, we raised the temperature to 800 K for 1 ns, then cooled it down for 1 ns at 550 K and equilibrated at 550 K for 2 ns. Once the system is at equilibrium at 550 K we performed a 1 ns acquisition followed by 1 ns of cooling down to 540 K and 1 ns of equilibration and 1 ns acquisition. This process is performed until we reach a temperature of 240 K, using a 10 K step. For each temperature the density of the system is calculated. Figure 1 shows the specific volume as a function of the temperature, we can see an inflection in the plot which gives two regions, the $T_g$ is taken as the intercept of the linear fits of these two regions.

However, in order to compare the simulation versus the experimental values, the re-

lation of Williams-Landel-Ferry,[62] (equation 13), which relies on the principle of time-temperature equivalence is applied,

$$\log_{10} \alpha_t = \log_{10} \frac{q_{exp}}{q_{simu}} = \frac{-C_1(T_{\text{g, shifted}} - T_{\text{g, exp}})}{C_2 + T_{\text{g, shifted}} - T_{\text{g, exp}}}, \tag{13}$$

were $q_{exp}$ and $q_{simu}$ are the cooling rates of the experiment and the simulation, respectively. In our case $q_{exp} = 20\,\text{K}\,\text{min}^{-1}$ and $q_{simu} = 5\,\text{K}\,\text{ns}^{-1}$. We use the universal constants, $C_1$ and $C_2$ (with $C_1 = 17.44$ and $C_2 = 51.6\,\text{K}$), because it would be time-consuming to fit our own constant.[63] Graphically, we obtained $T_\text{g}$=415 K. By applying equation 13, and using the default parameters, we obtained a shifted glass transition temperature for our simulation result of $T_{\text{g,simulation, shifted}} = 328\,\text{K}$. The difference between our experimental and simulated glass transition temperatures is less than 7% and both of them are in good agreement with other results previously published.[58–60] Hence, it could be concluded that our model for the PET reproduces correctly its glass transition temperature. From this calculations, we also obtain a density of amorphous PET at 300 K of $1.316\,\text{g}\,\text{cm}^{-3}$, which is in good agreement with previous results.[58–60]

Using the eight previous systems at 300 K, we can calculate the mass of entanglement ($M_e$). This property describes the average molecular weight of polymer chains between two consecutive junctions. Experimentally, for PET, this mass is between 1450 and $2250\,\text{g}\,\text{mol}^{-1}$, with an average at $1700\,\text{g}\,\text{mol}^{-1}$,[64] which would be equal to a number of entanglement between 1.28 and 1.98 per chain, respectively. To calculate $M_e$ of our system we used the primitive path analysis (PPA) method,[65] which has been implemented for LAMMPS output files.[66] After equilibration at 300 K and 2 ns of acquisition we find an average entanglement of 1.90 per chain which is consistent with experiments. Therefore, our systems are representative of a real polymer melt, by reproducing correctly three meaningful properties of polymers such as density, $T_\text{g}$ and $M_e$.

We turn now our attention to the reproduction of the Young modulus of PET. The

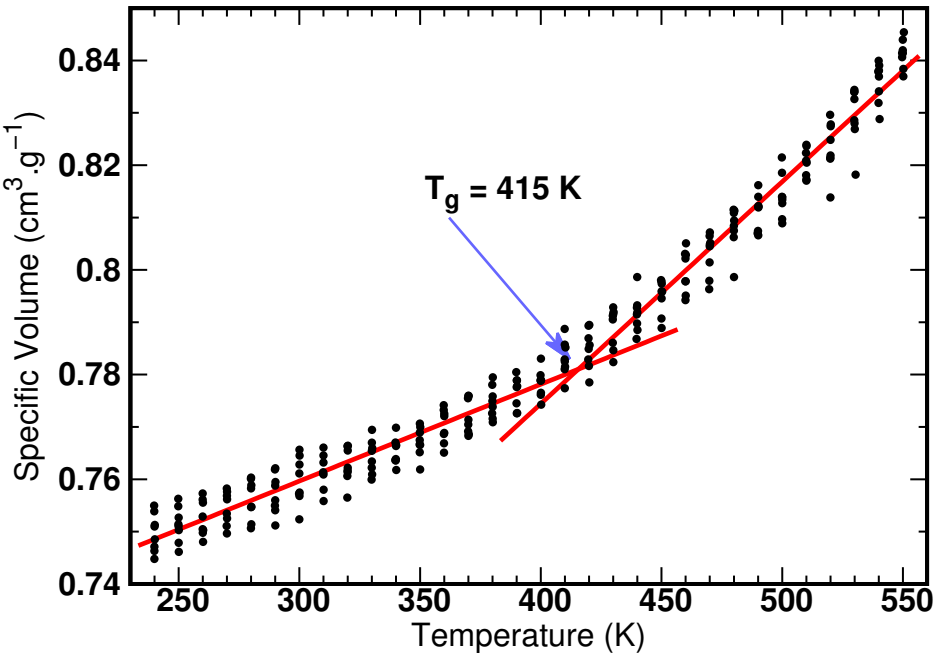


Figure 1: Specific volume of PET with respect to the temperature. The glass transition temperature is considered as the intersection of the two red lines. The densities of the eight independent structures are reported here for each temperature.

Young's modulus can be obtained experimentally by a traction test . One way to calculate this property by MD simulation has been proposed using a method based on the fluctuation of local density.[67] Consequently, a constant NVT simulation was performed during 2 ns at 300 K for each system. The predicted elastic properties by MD simulation with PCFF+ force field of PET at 300 K are given in Table 1. We can see that our results are in good agreement with both previous results[68] and experiments.[69–71] The Young's modulus (E), the bulk modulus and the Poisson's ratio are very close to the values measured and calculated in other works.[68] The value obtained for the Young's modulus is very satisfactory, and matches very well with experiments. This reinforces our confidence in the choice of the force field for the extraction of a monomer from the bulk.

**Table 1: Young's modulus (E), bulk modulus (K), and Poisson's ratio ($\nu$) of PET at 300 K.**

| Properties (GPa) | E | K | $\nu$ |
|---|---|---|---|
| Our results | 3.20 | 8.30 | 0.43 |
| Experiment[69–71] | 3.00 | 6.30 | 0.43 |
| Simulation[68] | 2.70 | 6.43 | 0.43 |

## 4.2 Extraction of a monomer from PET

In this section, we aim to model a process that helps us in the understanding of enzymatic degradation of polymer through the calculation of a potential of mean force of a monomer by the Umbrella Sampling (US) method. Figure 2 represents two visualizations of the final state of the system at the end of the US calculations in water and ethylene glycol. Figure

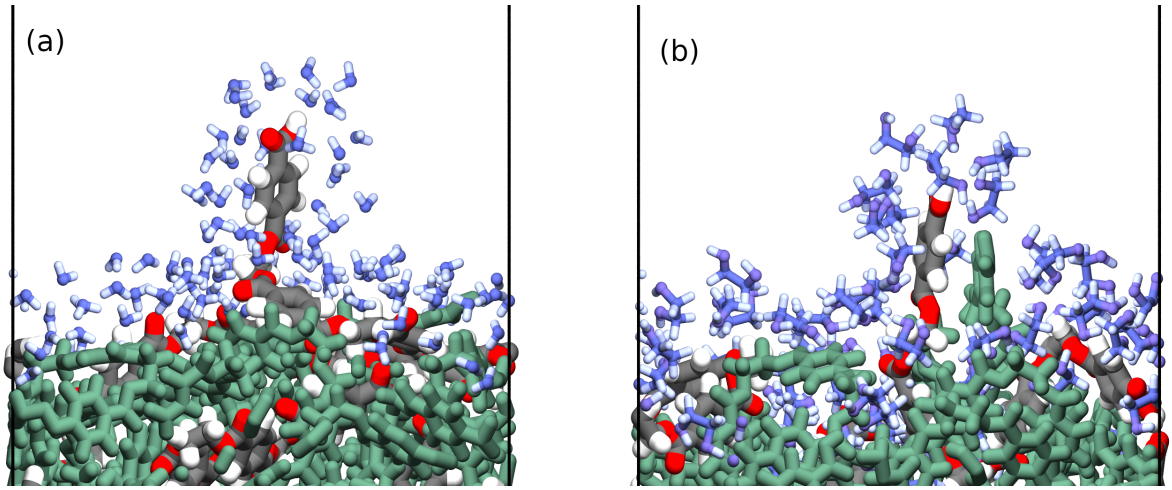


Figure 2: Molecular visualizations of the final structure after performing the chain extraction of PET in (a) water and in (b) ethylene glycol. Polymer chains are shown in dark green, the chain subjected to the pull-out is shown in colors, red is used for oxygen atoms, black for carbon atom and white for hydrogen atoms. In both pictures, only the solvent molecules within 5 Å of the pulled chain are shown in blue for clarity.

2b, shows that in the case of using ethylene glycol as solvent, some of the solvent molecules diffuse into the polymer, and therefore, weaken the polymer-polymer interaction and make it easier to extract a chain from the bulk. This phenomena is not observed in the PET-water system. Beside, for the PET-ethylene glycol system, a chain from the bulk "follows" the

chain subjected to the PMF. We have to be careful here, because this event can be a rare event only happening in this simulation with this specific configuration.

Following we develop a more quantitative analysis of these system. Figure 3 shows the profiles of the Gibbs free energy as a function of the $z$-separation distance between the end of the polymer chain (the hydrogen atom) and the center of mass of the polymer bulk (without considering the chain in tension). In all simulations, we systematically start with the same configuration of the polymer melt and after equilibration, we extract the same chain. In this way we can compare the results between all the solvents. We pull-out a chain which ends at the surface after equilibration. To summarize, at the end of our equilibration (in all solvents), the same chain end is near the surface. We apply the US potential to the final hydrogen of this chain relative to the center of mass of all other chains. We perform the extraction of this chain over a length of 10 Å, which represents the length of a monomer, with a step of 0.1 Å, and a simulation time of 0.25 ns for each step. This gives us a US simulation of 25 ns for each solvent considered. The management of the US is done via the COLVARS module package[56] which manages the potential that restricts the distance between the two centers of mass. It is impossible to perform this calculation in both directions, because once the monomer is extracted the rearrangement of the chains in the bulk does not allow the inverse transformation. As shown in Figure 3, for all the considered solvents, water, ethylene glycol, dodecane and vacuum, we observe a positive $\Delta$G, ranging between 10 and 44 kJ mol$^{-1}$. This results clearly shows that it is not energetically favorable to extract a polymer chain from PET. Let us first compare the profiles between water and vacuum. The energy needed to extract a monomer into water from the bulk is about 44 kJ mol$^{-1}$, which is the most unfavorable among all the environment tested here, whereas in the case of vacuum it is about 23 kJ mol$^{-1}$. This means, it is almost twice more energy demanding to extract a monomer into water than vacuum. If we look closely at Figure 3, we can see that even to extract half the monomer ($z = 5$ Å) into water needs a significant free energy cost about 40 kJ mol$^{-1}$. The stronger free energy cost in water than in vacuum is explained

by the disruption of hydrogen bond of water on the surface of PET in the region of the monomer. The reorganization of the hydrogen bond network is very costly from an free energy viewpoint. This result was expected from the uses of PET, which is mainly used for food container and more specifically plastics bottle for drinking water. If some monomers could partially diffuse into the water, this will lead to a natural degradation of the polymer on the long term.

We now focus on the extraction of PET chain into dodecane as a nonpolar solvent. The energy required to extract the monomer, is about $19\,\mathrm{kJ\,mol^{-1}}$, which is lower than that needed in the void. The extraction of a PET chain into ethylene glycol is still unfavorable, but its only requires $10\,\mathrm{kJ\,mol^{-1}}$ at $300\,\mathrm{K}$, which means it is probably less at higher temperature. It is also four times less than the energy needed to extract the same monomer into water. Extracting a monomer into the ethylene glycol is more favorable than into water, the energy for the vacuum and dodecane are in-between. It could be concluded that, as the enzymatic

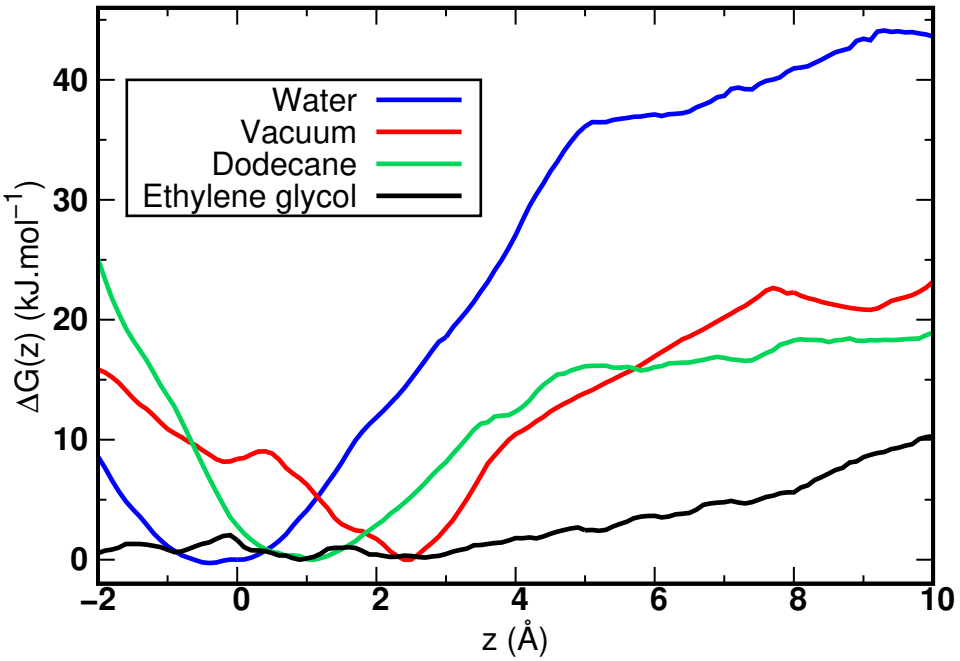


Figure 3: Free energy profiles of the chain as a function of the distance between the hydrogen at the end of the chain and the center of mass of the PET, for the amorphous system. In this figure $z = 0$ represents the initial position of the hydrogen atom.

degradation is taking place, the concentration of ethylene glycol increases. Therefore, it is

easier for the enzyme to extract a chain from the bulk. To conclude this first analysis, we can say that whatever the solvent considered in this study, it is not energetically favorable to extract a monomer from the bulk of the polymer. Thus, it can be stated that an enzymatic degradation will occur only if the enzyme bonds closely to the surface of PET. The catalytic site must provide an environment more favorable for the monomer than the one provided by the bulk.

Other questions may arise from these results : when the traction of a chain is happening, are the chains in the close vicinity undergoing a conformational change that would modify the state of the polymer surface and thus lead to a modification of the PET solvent interactions? Even if Figure 2 makes a partial contribution to the answer of this question, we propose here to investigate the modification of the surface between the initial configuration and its final state when the monomer is extracted into water or ethylene glycol. To do this, we calculated the intrinsic density profile in two dimensions using the Identification of Truly Interfacial Molecules (ITIM) method.[72–75] The first step of the ITIM method is to detect the set of true interfacial atoms of the considered surface. These atoms are spotted by a program which generates a series of probe spheres moving along the z direction along a grid of test lines. These profiles are obtained by using the equation 14:

$$\rho(z') = \left\langle \frac{1}{A} \sum_{i=1}^{N} \delta(z - z_i + \xi(x_i, y_i)) \right\rangle, \tag{14}$$

where $\rho(z')$ is the intrinsic density profile, $N$ is the number of atoms to be considered, $A$ is the surface area, $z_i$ is the $z$-position of the atom $i$, $\delta$ is the Dirac delta function, $\xi$ is the instantaneous position of the surface and $x_i$ and $y_i$ are the atomic coordinates in the plane parallel to the interface. We chose a probe of diameter 3.5 Å which is the size of a water molecule in terms of van der Waals diameter. We used a 120 $\times$ 120 grid, which allows for a fast calculation as well as a sufficiently high resolution of 0.275 Å given the box dimensions along the $x$ and $y$ directions. The two-dimensional profiles for water and ethylene glycol are shown in Figure 4. Figure 4a shows the intrinsic density of the PET surface before

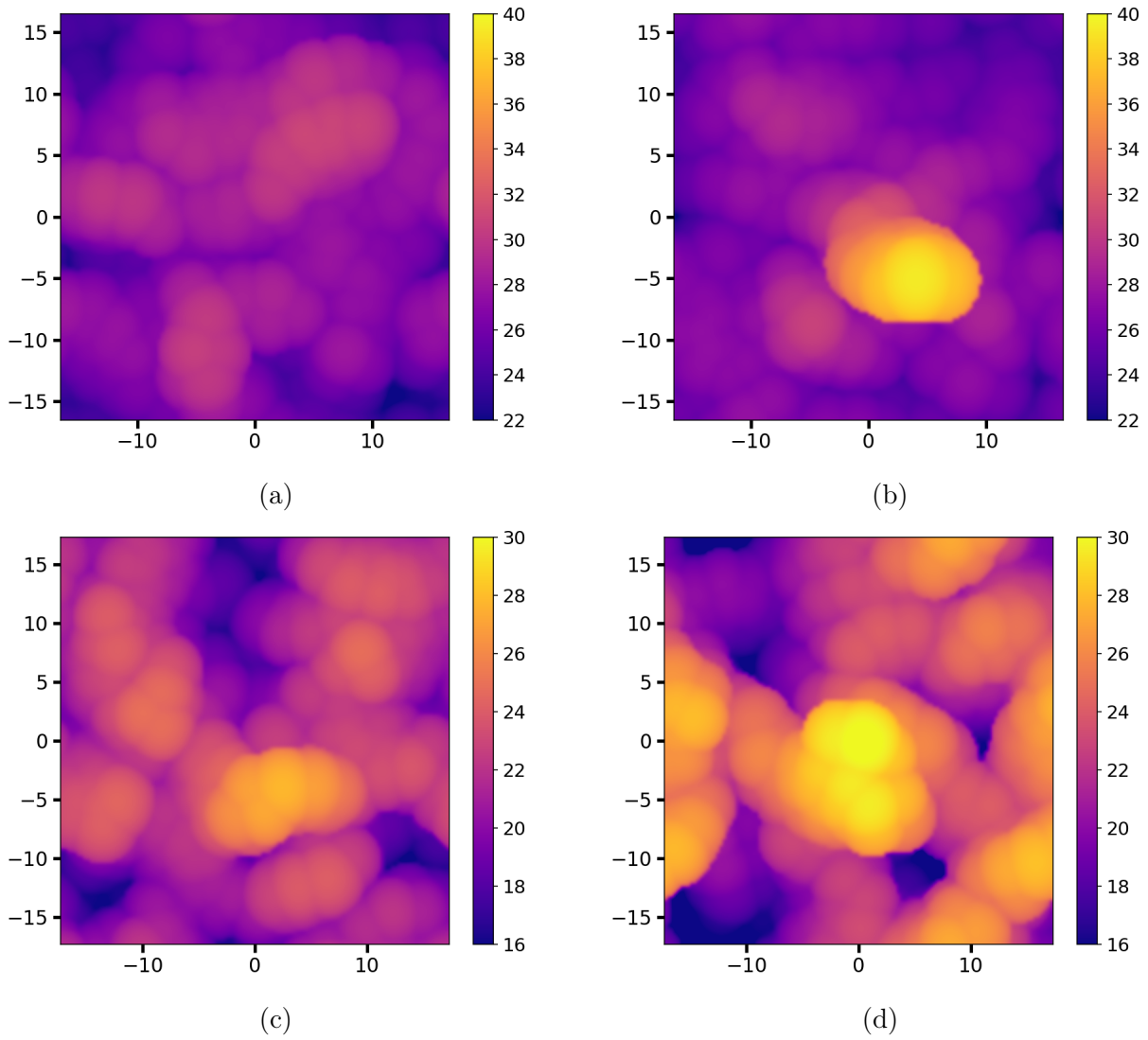


Figure 4: Intrinsic 2D density profiles calculated at two different stages of the US simulation in water (a, b) and ethylene glycol (c, d) for the initial configuration (a, c) and the final one after extracting a monomer (b, d).

the traction of the monomer takes place, and Figure 4b shows the intrinsic density of the PET surface when the monomer is fully extracted from the bulk into water. In each of the presented figures, the atom subjected to traction is located at the center of the plot. The intrinsic density in this case can be assimilated to the surface roughness. We can observe, by comparison of the two images, that according to the color code used (the brighter the color the higher the position of the atom), there is no disturbance at short and long distance of the chains surrounding the chain tracted. If this monomer get extracted from the bulk, and

be cut by the enzyme, the quantity of energy needed to extract another monomer, would be independent of the previous degradation. For the PET-EG system, comparison of Figure 4c and Figure 4d shows that the areas of the image in Figure 4d appear in yellow, (which means a higher positions along $z$), were more numerous after extraction. This confirms the visual observation made in Figure 2b. In addition to the chain accompanying the towed chain, we can observe that the position of the chains located at the edge of the box has also been changed along the z axis. This shows that the presence of ethylene glycol has a disruptive effect onto the polymer surface and increasing its concentration will probably promotes enzymatic degradation.

By using ITIM method,[72–75] we calculate the density intrinsic profiles between the solvent (water, ethylene glycol, dodecane) and the PET surface. The density profiles calculated and presented in Figure 5 consider the surface roughness. Figure 5a, which represents the density profile of PET-water, shows that there is no penetration of water molecules inside the polymer, and the first 5 Å layer of water molecules in contact with the PET is structured. If we now compare Figure 5a and Figure 5b, it can be observed that, as for water, ethylene glycol is structured by the presence of the surface over a distance of 8 Å. However, unlike water, there is a clear penetration of the ethylene glycol molecules into the PET surface, creating a zone where a partial mixing between the polymer and the solvent occurs. This confirms, the previous results, (PMF and 2D density profile), that ethylene glycol induces a disruption and a local rearrangement of the polymer chains on the surface, during the chain extraction. In this case, the interfacial region is composed of ethylene glycol molecules and monomers. The same observations made for the ethylene glycol can be transferred to the dodecane as illustrated in Figure 5c. We observe that the solvent is structured over a distance of 8A, as well as a penetration of it into the polymer matrix.

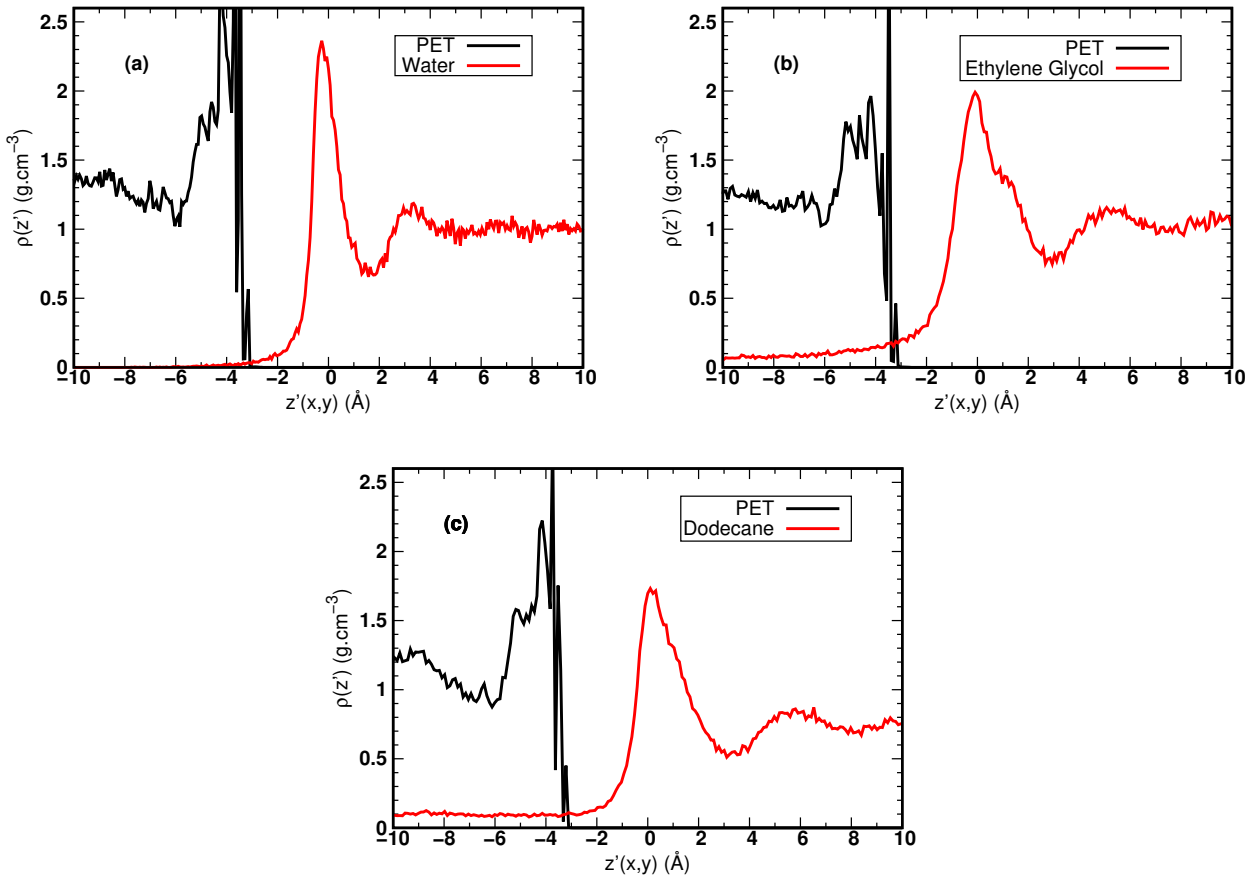


Figure 5: Intrinsic density profiles calculated for the adsorption of water (a) ethylene glycol (b) and dodecane (c) onto the amorphous PET surface.

## 4.3 Work of adhesion of PET-water

For a better understanding of the enzymatic catalysis that will start in water, we need to evaluate energy contributions between PET and water. The work of adhesion is a key-property in this process since it is the result of a balance between the different interfacial tensions occurring at the interface. Experimentally, the work of adhesion can be determined via the contact angle. Indeed, the contact angle of a water droplet onto an amorphous PET surface is about 83.5°.[76] By considering the surface tension $\gamma_{SV}$ for the PET of about 45.6 mJ m$^{-2}$ [76] and the liquid-vapor surface tension of water $\gamma_{LV}$ at 71.8 mJ m$^{-2}$, we can estimate the work of adhesion at 79.9 mJ m$^{-2}$ and the solid-liquid surface tension $\gamma_{SL}$ at 37.4 mJ m$^{-2}$. In this work, we measured the contact angle of water droplet on the PET

plate. This angle was determined to 72.3° which gives an experimental work of adhesion of $93.6\,\mathrm{mJ\,m^{-2}}$. Even if the experimental values may be a little different, they can guide the molecular simulations on the order of magnitude of the values to be obtained but also on the difficulty and therefore the experimental uncertainty related to these measurements.

First, we have to determine the value of $\gamma_{\mathrm{LV}}$ for the force field used for water. The surface tension of liquid-vapor[77] for the TIP4P/2005 water model has been extensively calculated : we retain the value of $\gamma_{\mathrm{LV}} = 72.0\,\mathrm{mJ\,m^{-2}}$ calculated by Goujon et al.[78] This model gives a surface tension value that is very close to the experimental value.[79]

We start by calculating the solid-liquid work of adhesion between the PET and water, for an amorphous and crystalline form of polymers. The amorphous system consists of 12 chains of polymer of 15 monomers and 1000 water molecules. For the crystalline system, a 10×7×9 cell has been generated from the crystalline structure of PET with 2000 water molecules. PET is crystallised under one form, triclinic, and in all simulations we used the (100) surface of the crystal lattice.[80] The results of the solid-liquid work of adhesion with the FEP method for both systems are presented in Figure 6. We obtained a work of adhesion of 85.4 and $85.7\,\mathrm{mJ\,m^{-2}}$ for the amorphous and the crystalline systems respectively. For the amorphous system it leads to a contact angle of 79.2° which is between the experimental values reported in this section. The crystalline system gives a contact angle of 79.0° but the comparison with the corresponding experimental property is not possible. We can only compare this result with that of a MD simulation of crystalline PET.[41] A contact angle of 102.0° was found, however this result has to be taken cautiously, because it was the result of a direct measurement of the angle form by a nanodroplet made up of a small number of water molecules (216). Additionally, in this study, the PET surface was kept fixed, the size of the water droplet, and the effects of line tension were not considered. As we obtained different results with the PMF of a monomer in dodecane, we also calculated the work of adhesion of dodecane on PET. Experimentally, we observe a complete spreading of the droplet onto the surface. This indicates that the work of adhesion is maximum in the case

of dodecane. Using MD simulations, we calculated a solid-liquid work of adhesion between the PET and the dodecane. The composition of amorphous and crystalline PET were the same, and we used 150 and 300 dodecane molecule for the amorphous and crystalline system respectively. We obtained a work of adhesion of 85.3 and 86.1 $\mathrm{mJ\,m^{-2}}$ for the amorphous and the crystalline systems respectively. The experimental liquid-vapor surface tension of dodecane is about $\gamma_{\mathrm{LV}} = 23.8\,\mathrm{mJ\,m^{-2}}$.[81] Using this result and equation 4, we obtained a value for cos $\theta$ greater than 1, meaning that the solid-liquid work of adhesion PET-dodecane is maximum. These results agree with the experimental observations.

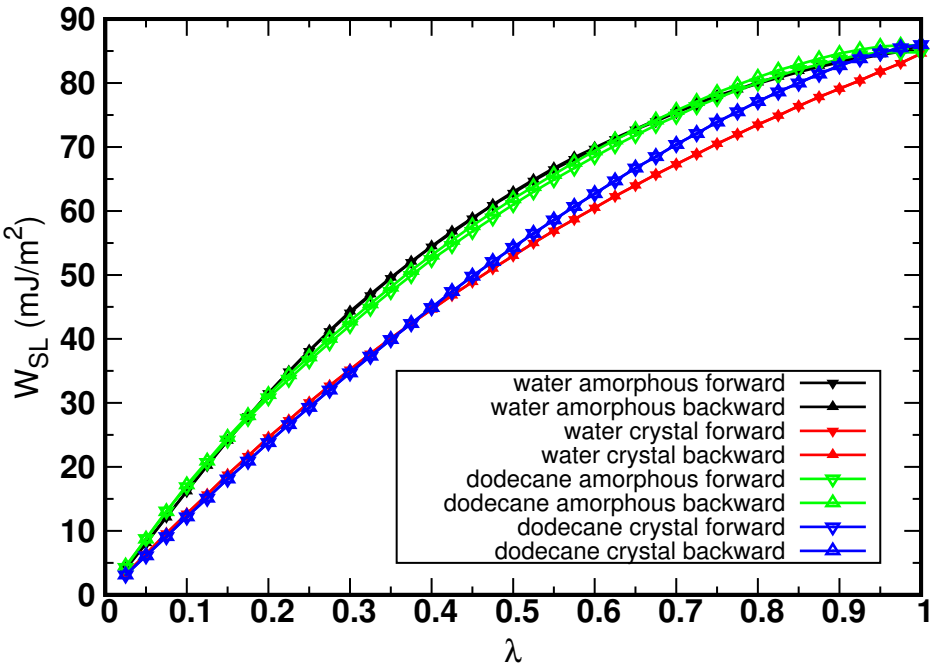


Figure 6: Cumulative work of adhesion in the forward and backward directions, of water (amorphous black and crystal red) and dodecane (amorphous green and crystal blue) onto a PET surface as a function of the coupling parameter $\lambda$ for 40 windows and during 10 ns of MD simulation. The value of the work of adhesion is read at $\lambda = 1$.

## 4.4 Water nanodroplet interacting with PET

In order to complement the results obtained with the free energy perturbations on the calculation of $W_{\mathrm{SL}}$, we propose here to address the direct calculation of the contact angle of a nanodroplet onto PET polymer surfaces. We also examined the impact of the droplet size

on the value of the contact angle at the molecular scale. In order to calculate the contact angle between a water droplet and a PET surface via molecular simulations, we created an amorphous slab of polymer composed of 300 chains of 15 monomers, which gives a block of $L_x = L_y = 172.0\,\text{Å}$ and $L_z = 41\,\text{Å}$. For the crystalline system we built a 34×19×10 supercell of (100) PET, which is about 200 Å for $L_x$ and $L_y$, and 30 Å for $L_z$ direction. To evaluate the macroscopic contact angle using the equation 12, which describes the size dependence of microscopic droplets, we simulated systems comprising of 500, 1200, 3000, 6000 and 18 000 water molecules for 4 ns. We saved the trajectories of the system every 1000 steps, which give us 4000 configurations to analyse. We determined the contact angle by fitting a spherical cap on the water density by using maximum likehihood method.[52] Using the values obtained from these independent simulations we calculated the macroscopic angle and the line tension $\tau$ (see equation 12). Figure 7a represents the values of $\cos\theta_\mu$ as a function of $1/r_d$ for different droplet sizes onto PET. Figure 7b also represents the evolution of the angle as a function of the radius of the droplet. Figure 7a allows to calculate $\theta$ for a macroscopic droplet and

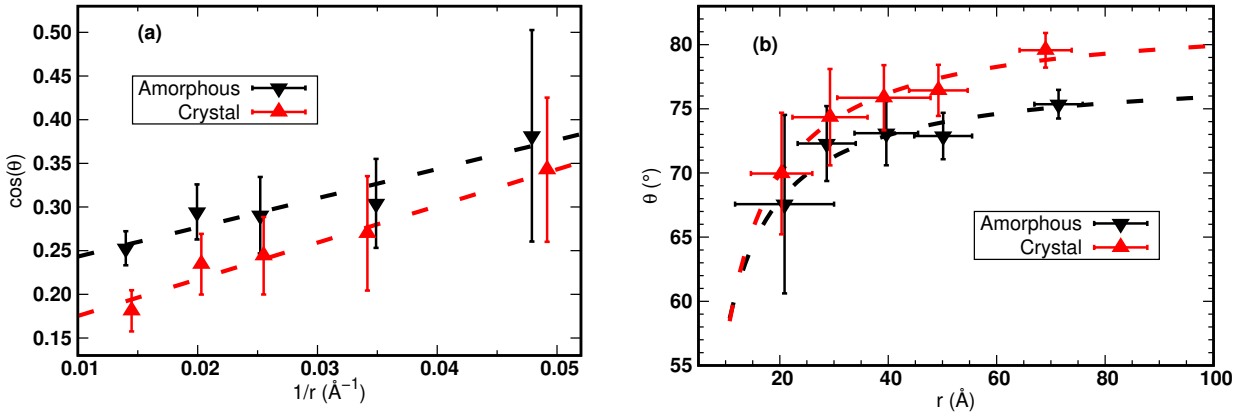


Figure 7: (a) Measurement of the cosine of the contact angle of water nanodroplets wetting PET surfaces as a function of the inverse of the radius of contact $r_d$, for amorphous and crystal systems. The dashed line represent the fitted curves used to calculate $\theta_\mu$. (b) Contact angle as a function of $r_d$ for the amorphous (black) and crystalline (red) PET surfaces. The macroscopic contact angles $\theta_\mu$ were calculated by extrapolating $\cos\theta$ to $1/r_d = 0$ from Figure 7a.

the value of $\tau$ by applying a simple linear fit. We find a value of $\cos\theta = 0.209$ which gives

a value for the contact angle onto an amorphous surface of 77.8° and $\cos\theta = 0.133$ and a contact angle of $\theta = 82.3°$ for the crystalline phase. These values are in good agreement with the experimental data and FEP results listed in the previous section. The linear regression gives values for both phases a negative line tension $\tau$ of $-2.4 \times 10^{-11}\,\mathrm{J\,m^{-1}}$ and of $-3.1 \times 10^{-11}\,\mathrm{J\,m^{-1}}$, for the amorphous and crystal phase respectively. These values are in the same range as calculated line tensions for linear polymers.[42,44] We can conclude that both methodologies consisting in calculating the contact angle by modelling an explicit droplet and in calculating the work of adhesion match very well. These advanced methodologies inform about the strength of the interaction between the PET polymer surface and water molecules.

# 5 Conclusion

Our aim was to gain a better understanding of the energetics of the PET depolymerization. Before investigating the enzymatic degradation of PET which will require more significant computing resources and a multi-scale approach, it was essential to check the performance of the force field and methodology to investigate structural and thermodynamic properties of the PET-water interface. The use of more sophisticated methods for investigating the extraction of a monomer from the PET surface,calculating the work of adhesion and the contact angle allows us to characterize energetically some interfacial properties which could be critical in the energy balance of the enzymatic degradation of PET.

From a functional point of view, the PCFF+ force field was shown to reproduce accurately the density, the mass of entanglement, the glass transition temperature and Young's modulus of PET. As a matter of fact, MD simulations predicted a glass transition temperature of 328 K which deviates by only 7% from experiments, an average entanglement of 1.9 per chain and a density of amorphous PET of $1.316\,\mathrm{g\,cm^{-3}}$ at 300 K. The simulated Young modulus of 3.0 GPa was found to match very weel with the corresponding experimental property. We

used the potential of mean force approach and the Umbrella Sampling method to study the extraction of a monomer from the PET to different media such as water, dodecane, ethylene glycol and vacuum. First, it was established that the required free energy is always positive regardless of the environment.The most unfavourable extraction is obtained in water with a free energy cost of about $44\,\mathrm{kJ\,mol^{-1}}$. This high cost compared to vacuum is explained by the reorganization of hydrogen bond network close to the PET surface around the area where the monomer is extracted. This allows us to assert that the placement of the polymer in the active site of the enzyme can only be done if the latter provides an environment as favorable as the one provided by the bulk. In other terms, the chemical affinity between the enzyme and the polymer should be, at least, the same as the polymer-polymer affinity. Intensive calculations of potential of mean force between the enzyme and the PET could be considered in the near future but such simulations represent an important computational challenge because of the size of the enzyme and the degree of freedoms to be considered for the calculation of the free energy of adsorption. In order to avoid an excessive energy cost, it is reasonable to assume that the enzyme must be in contact with the surface for it to be degraded. Indeed, at the beginning of the traction in water over the first two angstroms, the required energy is of the order of $10\,\mathrm{kJ\,mol^{-1}}$. From a structural point of view, if the extraction of a bulk chain is softly done, we observed then that the surrounding polymer chains were not impacted.

All of these results motivated us to deeply study the solid-solvent interactions, which are described experimentally by measuring the surface tension. Therefore, we calculated the work of adhesion of water and the macroscopic contact angle. The simulated work of adhesion was found to be equal to $93.6\,\mathrm{mJ\,m^{-2}}$ and the modelling of a water nanodroplet on PET yielded a contact angle of about $78^\circ$ which compared very well with thoses deduced from the work of adhesion and experiments. We showed that we can reproduced correctly the energetics of the PET-water interface by using free energy methods. To finish, this study is a first step toward understanding the processes involved in the catalytic reaction of the

degradation of PET by an enzyme. We are continuing this investigation, by simulating the enzyme and its affinity with PET through a very demanding calculation of potential of mean force. However, the work reported here provided us some fundamental answers regarding the complex subject of enzymatic degradation and the interaction between PET and water.

# ACKNOWLEDGMENTS

This work was performed in SimatLab, a joint public-private laboratory dedicated to the modeling of the polymer materials. This laboratory is supported by Michelin, Clermont Auvergne University (UCA), CHU of Clermont-Ferrand and CNRS. We are also grateful to the Mésocentre Clermont Auvergne University for providing computing and storage resources. This work was performed using HPC resources from GENCI-IDRIS (Grant AD010913369). We gratefully thanks Dr Mehdi Sahihi for proofreading the manuscript.

# References

(1) Geyer, R.; Jambeck, J. R.; Law, K. L. Production, use, and fate of all plastics ever made. *Sci. Adv.* **2017**, *3*, e1700782.

(2) Frounchi, M. Studies on degradation of PET in mechanical recycling. Macromol. Symp. 1999; pp 465–469.

(3) Ragaert, K.; Delva, L.; Van Geem, K. Mechanical and chemical recycling of solid plastic waste. *Waste Manage.* **2017**, *69*, 24–58.

(4) Spychaj, T. *Chemical recycling of PET: methods and products*; Wiley Online Library, 2002; pp 1252–1290.

(5) Khoonkari, M.; Haghighi, A. H.; Sefidbakht, Y.; Shekoohi, K.; Ghaderian, A. Chemical recycling of PET wastes with different catalysts. *Int. J. Polym. Sci.* **2015**, *2015*.

(6) Fischer-Colbrie, G.; Heumann, S.; Liebminger, S.; Almansa, E.; Cavaco-Paulo, A.; Guebitz, G. M. New enzymes with potential for PET surface modification. *Biocatal. Biotransform.* **2004**, *22*, 341–346.

(7) Then, J.; Wei, R.; Oeser, T.; Barth, M.; Belisário-Ferrari, M. R.; Schmidt, J.; Zimmermann, W. $Ca^{2+}$ and $Mg^{2+}$ binding site engineering increases the degradation of polyethylene terephthalate films by polyester hydrolases from Thermobifida fusca. *Biotechnol. J.* **2015**, *10*, 592–598.

(8) Eberl, A.; Heumann, S.; Brückner, T.; Araujo, R.; Cavaco-Paulo, A.; Kaufmann, F.; Kroutil, W.; Guebitz, G. M. Enzymatic surface hydrolysis of poly (ethylene terephthalate) and bis (benzoyloxyethyl) terephthalate by lipase and cutinase in the presence of surface active molecules. *J. Biotechnol.* **2009**, *143*, 207–212.

(9) Oeser, T.; Wei, R.; Baumgarten, T.; Billig, S.; Föllner, C.; Zimmermann, W. High level expression of a hydrophobic poly (ethylene terephthalate)-hydrolyzing carboxylesterase from Thermobifida fusca KW3 in Escherichia coli BL21 (DE3). *J. Biotechnol.* **2010**, *146*, 100–104.

(10) Jia, Y.; Samak, N. A.; Hao, X.; Chen, Z.; Yang, G.; Zhao, X.; Mu, T.; Yang, M.; Xing, J. Nano-immobilization of PETase enzyme for enhanced polyethylene terephthalate biodegradation. *Biochem. Eng. J.* **2021**, *176*, 108205.

(11) Tokiwa, Y.; Suzuki, T. Hydrolysis of polyesters by lipases. *Nature* **1977**, *270*, 76–78.

(12) Tournier, V.; Topham, C.; Gilles, A.; David, B.; Folgoas, C.; Moya-Leclair, E.; Kamionka, E.; Desrousseaux, M.-L.; Texier, H.; Gavalda, S. et al. An engineered PET depolymerase to break down and recycle plastic bottles. *Nature* **2020**, *580*, 216–219.

(13) Silva, C.; Da, S.; Silva, N.; Matamá, T.; Araújo, R.; Martins, M.; Chen, S.; Chen, J.; Wu, J.; Casal, M. et al. Engineered Thermobifida fusca cutinase with increased activity on polyester substrates. *Biotechnol. J.* **2011**, *6*, 1230–1239.

(14) Yoshida, S.; Hiraga, K.; Takehana, T.; Taniguchi, I.; Yamaji, H.; Maeda, Y.; Toyohara, K.; Miyamoto, K.; Kimura, Y.; Oda, K. A bacterium that degrades and assimilates poly (ethylene terephthalate). *Science* **2016**, *351*, 1196–1199.

(15) Austin, H. P.; Allen, M. D.; Donohoe, B. S.; Rorrer, N. A.; Kearns, F. L.; Silveira, R. L.; Pollard, B. C.; Dominick, G.; Duman, R.; El Omari, K. et al. Characterization and engineering of a plastic-degrading aromatic polyesterase. *Proc. Natl. Acad. Sci.* **2018**, *115*, E4350–E4357.

(16) Coburn, J. C.; Boyd, R. H. Dielectric relaxation in poly (ethylene terephthalate). *Macromolecules* **1986**, *19*, 2238–2245.

(17) Marten, E.; Müller, R.-J.; Deckwer, W.-D. Studies on the enzymatic hydrolysis of polyesters. II. Aliphatic–aromatic copolyesters. *Polym. Degrad. Stab.* **2005**, *88*, 371–381.

(18) Ronkvist, Å. M.; Xie, W.; Lu, W.; Gross, R. A. Cutinase-catalyzed hydrolysis of poly (ethylene terephthalate). *Macromolecules* **2009**, *42*, 5128–5138.

(19) Joo, S.; Cho, I. J.; Seo, H.; Son, H. F.; Sagong, H.-Y.; Shin, T. J.; Choi, S. Y.; Lee, S. Y.; Kim, K.-J. Structural insight into molecular mechanism of poly (ethylene terephthalate) degradation. *Nat. Commun.* **2018**, *9*, 382.

(20) Boneta, S.; Arafet, K.; Moliner, V. QM/MM study of the enzymatic biodegradation mechanism of polyethylene terephthalate. *J. Chem. Inf. Model.* **2021**, *61*, 3041–3051.

(21) Zheng, M.; Li, Y.; Dong, W.; Feng, S.; Zhang, Q.; Wang, W. Computational biotransformation of polyethylene terephthalate by depolymerase: A QM/MM approach. *J. Hazard. Mater.* **2022**, *423*, 127017.

(22) Zheng, M.; Li, Y.; Xue, R.; Dong, W.; Zhang, Q.; Wang, W. Hydrolases catalyzed

nanosized polyethylene terephthalate depolymerization: New insights from QM/MM analysis. *J. Clean. Prod.* **2022**, *377*, 134429.

(23) Charupanit, K.; Tipmanee, V.; Sutthibutpong, T.; Limsakul, P. In silico identification of potential sites for a plastic-degrading enzyme by a reverse screening through the protein sequence space and molecular dynamics simulations. *Molecules* **2022**, *27*, 3353.

(24) Sangkhawasi, M.; Remsungnen, T.; Vangnai, A. S.; Poo-arporn, R. P.; Rungrotmongkol, T. All-atom molecular dynamics simulations on a single chain of PET and PEV polymers. *Polymers* **2022**, *14*, 1161.

(25) Li, Q.; Zheng, Y.; Su, T.; Wang, Q.; Liang, Q.; Zhang, Z.; Qi, Q.; Tian, J. Computational design of a cutinase for plastic biodegradation by mining molecular dynamics simulations trajectories. *Comput. Struct. Biotechnol. J.* **2022**, *20*, 459–470.

(26) Lu, H.; Diaz, D. J.; Czarnecki, N. J.; Zhu, C.; Kim, W.; Shroff, R.; Acosta, D. J.; Alexander, B. R.; Cole, H. O.; Zhang, Y. et al. Machine learning-aided engineering of hydrolases for PET depolymerization. *Nature* **2022**, *604*, 662–667.

(27) Zuidema, H.; Waters, G. Ring method for the determination of interfacial tension. *Ind. Eng. Chem.* **1941**, *13*, 312–313.

(28) Hansen, F.; Rødsrud, G. Surface tension by pendant drop: I. A fast standard instrument using computer image analysis. *J. Colloid Interface Sci.* **1991**, *141*, 1–9.

(29) Good, R. J. Contact angle, wetting, and adhesion: a critical review. *J. Adhes. Sci. Technol.* **1992**, *6*, 1269–1302.

(30) MedeA®. Materials Exploration and Design Analysis, Materials Design, Inc., Angel Fire, NM, USA, 2016.

(31) Maple, J. R.; Dinur, U.; Hagler, A. T. New approaches to empirical force fields in review

of computational chemistry; 1991; Chapter 4.(b). *Proc. Natl. Acad. Sci. USA* **1988**, *85*, 5350.

(32) Sun, H.; Mumby, S. J.; Maple, J. R.; Hagler, A. T. An ab initio CFF93 all-atom force field for polycarbonates. *J. Am. Chem. Soc.* **1994**, *116*, 2978–2987.

(33) Abascal, J. L.; Vega, C. A general purpose model for the condensed phases of water: TIP4P/2005. *J. Chem. Phys.* **2005**, *123*, 234505.

(34) Young, T. III. An essay on the cohesion of fluids. *Philos. Trans. R. Soc. London* **1805**, 65–87.

(35) Leroy, F.; Müller-Plathe, F. Dry-surface simulation method for the determination of the work of adhesion of solid–liquid interfaces. *Langmuir* **2015**, *31*, 8335–8345.

(36) Zwanzig, R. W. High-temperature equation of state by a perturbation method. I. Nonpolar gases. *J. Chem. Phys.* **1954**, *22*, 1420–1426.

(37) Mezei, M.; Beveridge, D. Free energy simulations. *Ann. N. Y. Acad. Sci.* **1986**, *482*, 1–23.

(38) Ghoufi, A.; Malfreyt, P. Entropy and enthalpy calculations from perturbation and integration thermodynamics methods using molecular dynamics simulations: applications to the calculation of hydration and association thermodynamic properties. *Mol. Phys.* **2006**, *104*, 2929–2943.

(39) Chipot, C.; Pohorille, A. Free energy calculations. *Springer Ser. Chem. Phys.* **2007**, *86*, 159–184.

(40) Beutler, T. C.; Mark, A. E.; van Schaik, R. C.; Gerber, P. R.; Van Gunsteren, W. F. Avoiding singularities and numerical instabilities in free energy calculations based on molecular simulations. *Chem. Phys. Lett.* **1994**, *222*, 529–539.

(41) Fan, C. F.; Cağin, T. Wetting of crystalline polymer surfaces: A molecular dynamics simulation. *J. Chem. Phys.* **1995**, *103*, 9053–9061.

(42) Hirvi, J. T.; Pakkanen, T. A. Molecular dynamics simulations of water droplets on polymer surfaces. *J. Chem. Phys.* **2006**, *125*, 144712.

(43) Ambrosia, M. S.; Ha, M. Y.; Balachandar, S. The effect of pillar surface fraction and pillar height on contact angles using molecular dynamics. *Appl. Surf. Sci.* **2013**, *282*, 211–216.

(44) Kitabata, M.; Taddese, T.; Okazaki, S. Molecular dynamics study on wettability of poly (vinylidene fluoride) crystalline and amorphous surfaces. *Langmuir* **2018**, *34*, 12214–12223.

(45) Kitabata, M.; Taddese, T.; Okazaki, S. Wettability of a poly (vinylidene fluoride) surface by a pure good solvent and a good solvent/nonsolvent mixture: all-atom molecular dynamics study. *Langmuir* **2020**, *36*, 3633–3644.

(46) Scocchi, G.; Sergi, D.; D'Angelo, C.; Ortona, A. Wetting and contact-line effects for spherical and cylindrical droplets on graphene layers: A comparative molecular-dynamics investigation. *Phys. Rev. E* **2011**, *84*, 061602.

(47) Weijs, J. H.; Marchand, A.; Andreotti, B.; Lohse, D.; Snoeijer, J. H. Origin of line tension for a Lennard-Jones nanodroplet. *Phys. Fluids* **2011**, *23*, 022001.

(48) Pethica, B. The contact angle equilibrium. *J. Colloid Interface Sci.* **1977**, *62*, 567–569.

(49) Schimmele, L.; Napiórkowski, M.; Dietrich, S. Conceptual aspects of line tensions. *J. Chem. Phys.* **2007**, *127*, 164715.

(50) Giovambattista, N.; Debenedetti, P. G.; Rossky, P. J. Effect of surface polarity on water contact angle and interfacial hydration structure. *J. Phys. Chem. B* **2007**, *111*, 9581–9587.

(51) Hautman, J.; Klein, M. L. Microscopic wetting phenomena. *Phys. Rev. Lett.* **1991**, *67*, 1763.

(52) Orselly, M.; Devemy, J.; Bouvet, A.; Dequidt, A.; Loubat, C.; Malfreyt, P. Molecular interactions at the metal-liquid interfaces. *J. Chem. Phys.* **2022**, *156*, 234705.

(53) Plimpton, S. Fast parallel algorithms for short-range molecular dynamics. *J. Comput. Phys.* **1995**, *117*, 1–19.

(54) Nosé, S. A molecular dynamics method for simulations in the canonical ensemble. *Mol. Phys.* **1984**, *52*, 255–268.

(55) Martínez, L.; Andrade, R.; Birgin, E. G.; Martínez, J. M. PACKMOL: A package for building initial configurations for molecular dynamics simulations. *J. Comput. Chem.* **2009**, *30*, 2157–2164.

(56) Fiorin, G.; Klein, M. L.; Hénin, J. Using collective variables to drive molecular dynamics simulations. *Mol. Phys.* **2013**, *111*, 3345–3362.

(57) Reddish, W. The dielectric properties of polyethylene terephthalate (terylene). *Trans. Faraday Soc.* **1950**, *46*, 459–475.

(58) Hedenqvist, M.; Bharadwaj, R.; Boyd, R. Molecular dynamics simulation of amorphous poly (ethylene terephthalate). *Macromolecules* **1998**, *31*, 1556–1564.

(59) Boyd, S. U.; Boyd, R. H. Chain dynamics and relaxation in amorphous poly (ethylene terephthalate): A molecular dynamics simulation study. *Macromolecules* **2001**, *34*, 7219–7229.

(60) Eslami, H.; Müller-Plathe, F. Structure and mobility of poly (ethylene terephthalate): a molecular dynamics simulation study. *Macromolecules* **2009**, *42*, 8241–8250.

(61) NETZSCH, *Handbook DSC from NETZSCH*; Netzsch: Selb, Germany, 2015.

(62) Williams, M. L.; Landel, R. F.; Ferry, J. D. The temperature dependence of relaxation mechanisms in amorphous polymers and other glass-forming liquids. *J. Am. Chem. Soc.* **1955**, *77*, 3701–3707.

(63) Dudowicz, J.; Douglas, J. F.; Freed, K. F. The meaning of the "universal" WLF parameters of glass-forming polymer liquids. *J. Chem. Phys.* **2015**, *142*, 014905.

(64) Polymer database. `https://polymerdatabase.com/polymers/polyethyleneterephthalate.html`, (Accessed: April 6, 2022).

(65) Sukumaran, S. K.; Grest, G. S.; Kremer, K.; Everaers, R. Identifying the primitive path mesh in entangled polymer liquids. *J. Polym. Sci., Part B: Polym. Phys.* **2005**, *43*, 917–933.

(66) Maurel, G.; Schnell, B.; Goujon, F.; Couty, M.; Malfreyt, P. Multiscale modeling approach toward the prediction of viscoelastic properties of polymers. *J. Chem. Theory Comput.* **2012**, *8*, 4570–4579.

(67) Ikeda, A.; Berthier, L. Thermal fluctuations, mechanical response, and hyperuniformity in jammed solids. *Phys. Rev. E* **2015**, *92*, 012309.

(68) Latifa, B.; Zohra, F. F.; Said, H. Study of raw and recycled polyethylene terephthalate by meaning of TGA and computer simulation. *Adv. Polym. Technol.* **2020**, *2020*.

(69) Seitz, J. The estimation of mechanical properties of polymers from molecular structure. *J. Appl. Polym. Sci.* **1993**, *49*, 1331–1351.

(70) Ko, Y.-H.; Ahart, M.; Ko, J.-H.; Song, J. Investigation of polymorphism for amorphous and semi-crystalline poly (-ethylene terephthalate-) using high-pressure Brillouin spectroscopy. *J. Korean Phys. Soc.* **2017**, *70*, 382–388.

(71) Krevelen, D. W.; Hoftyzer, P.; Hoftyzer, P. *Properties of polymers, their estimation and correlation with chemical structure*; Elsevier Science & Technology, 1976.

(72) Pártay, L. B.; Hantal, G.; Jedlovszky, P.; Vincze, Á.; Horvai, G. A new method for determining the interfacial molecules and characterizing the surface roughness in computer simulations. Application to the liquid–vapor interface of water. *J. Comput. Chem.* **2008**, *29*, 945–956.

(73) Jorge, M.; Jedlovszky, P.; Cordeiro, M. N. D. A critical assessment of methods for the intrinsic analysis of liquid interfaces. 1. Surface site distributions. *J. Phys. Chem. C* **2010**, *114*, 11169–11179.

(74) Jorge, M.; Hantal, G.; Jedlovszky, P.; Cordeiro, M. N. D. A critical assessment of methods for the intrinsic analysis of liquid interfaces: 2. Density profiles. *J. Phys. Chem. C* **2010**, *114*, 18656–18663.

(75) Lapshin, D. N.; Jorge, M.; Campbell, E. E.; Sarkisov, L. On competitive gas adsorption and absorption phenomena in thin films of ionic liquids. *J. Mater. Chem. A* **2020**, *8*, 11781–11799.

(76) Wang, J.; Huang, N.; Yang, P.; Leng, Y.; Sun, H.; Liu, Z.; Chu, P. The effects of amorphous carbon films deposited on polyethylene terephthalate on bacterial adhesion. *Biomaterials* **2004**, *25*, 3163–3170.

(77) Goujon, F.; Malfreyt, P.; Boutin, A.; Fuchs, A. H. Vapour-liquid phase equilibria of n-alkanes by direct Monte Carlo simulations. *Mol. Simul.* **2001**, *27*, 99–114.

(78) Goujon, F.; Ghoufi, A.; Malfreyt, P. Associated molecular liquids at the graphene monolayer interface. *J. Chem. Phys.* **2021**, *154*, 104504.

(79) Pallas, N.; Harrison, Y. An automated drop shape apparatus and the surface tension of pure water. *Colloids Surf.* **1990**, *43*, 169–194.

(80) Kurita, T.; Fukuda, Y.; Takahashi, M.; Sasanuma, Y. Crystalline moduli of polymers,

evaluated from density functional theory calculations under periodic boundary conditions. *ACS OMEGA* **2018**, *3*, 4824–4835.

(81) Yang, J.; Wu, J.; Bi, S. Surface tension measurements by pendant drop method of 10 pure long-chain alkanes and alcohols for temperatures up to 573.15 K. *J. Chem. Eng. Data* **2021**, *66*, 2615–2628.

# TOC Graphic